2-7-2016

Improved Thermoelectric Performance of (Fe,Co)Sb_3-Type Skutterudites from First-Principles

Izaak Williamson
Boise State University

Logan Ju-Yee Her
Cosumnes River College

Xianli Su
Wuhan University of Technology

Yonggao Yan
Wuhan University of Technology

Winnie Wong-Ng
National Institute of Standards and Technology

See next page for additional authors

JOURNAL OF APPLIED PHYSICS **119**, 055101 (2016)

Improved thermoelectric performance of (Fe,Co)Sb_3-type skutterudites from first-principles

Izaak Williamson,[1] Logan Ju-Yee Her,[2] Xianli Su,[3] Yonggao Yan,[3] Winnie Wong-Ng,[4] and Lan Li[1,5]
[1]*Department of Materials Science and Engineering, Boise State University, Idaho 83725, USA*
[2]*Department of Science, Math and Engineering, Cosumnes River College, Sacramento, California 95823, USA*
[3]*State Key Laboratory of Advanced Technology for Materials Synthesis and Processing, Wuhan University of Technology, Wuhan 430070, China*
[4]*Materials Measurement Science Division, National Institute of Standards and Technology, Gaithersburg, Maryland 20899, USA*
[5]*Center for Advanced Energy Studies, Idaho Falls, Idaho 83401, USA*

(Received 9 September 2015; accepted 16 January 2016; published online 3 February 2016)

Skutterudite materials have been considered as promising thermoelectric candidates due to intrinsically good electrical conductivity and tailorable thermal conductivity. Options for improving thermal-to-electrical conversion efficiency include identifying novel materials, adding filler atoms, and substitutional dopants. Incorporating filler or substitutional dopant atoms in the skutterudite compounds can enhance phonon scattering, resulting in reduction of thermal conductivity, as well as improving electrical conductivity. The structures, electronic properties, and thermal properties of double-filled $Ca_{0.5}Ce_{0.5}Fe_4Sb_{12}$ and $Co_4Sb_{12-2x}Te_xGe_x$ compounds ($x = 0$, 0.5, 1, 2, 3, and 6) have been studied using density functional theory-based calculations. Both Ca/Ce filler atoms in $FeSb_3$ and Te/Ge substitution in $CoSb_3$ cause a decrease in lattice constant for the compounds. As Te/Ge substitution concentration increases, lattice constant decreases and structural distortion of pnictogen rings in the compounds occurs. This indicates a break in cubic symmetry of the structure. The presence of fillers and substitutions cause an increase in electrical conductivity and a gradual decrease in electronic band gap. A transition from direct to indirect band-gap semiconducting behavior is found at $x = 3$. Phonon density of states for both compounds indicate phonon band broadening by the incorporation of fillers and substitutional atoms. Both systems are also assumed to have acoustic-mode-dominated lattice thermal conductivity. For the $Co_4Sb_{12-2x}Te_xGe_x$ compounds, $x = 3$ has the lowest phonon dispersion gradient and lattice thermal conductivity, agreeing well with experimental measurements. Our results exhibit the improvement of thermoelectric properties of skutterudite compounds through fillers and substitutional doping. © *2016 AIP Publishing LLC*.
[http://dx.doi.org/10.1063/1.4940952]

INTRODUCTION

The combustion of fuel in automobiles is strikingly inefficient where approximately 75% of energy produced during this process is lost as waste heat. Thermoelectric materials can be used to recover some of this waste heat by converting it to useful electrical power for the vehicle. The performance of these materials is dictated by a dimensionless figure of merit defined as $ZT = S^2\sigma T/\kappa$, where the electrical properties are given in the "power factor" term ($S^2\sigma$), S being the Seebeck coefficient and σ being the electrical conductivity, and the thermal conductivity is given as κ. Materials with higher ZT values ($ZT > 1$) have greater thermoelectric performance. Such materials must exhibit a high power factor while having low thermal conductivity. In order to meet these criteria, it is important to identify novel materials or substitute existing materials with different species to optimize the ZT value.[1–11]

One class of materials that has potential for thermoelectric applications are skutterudite compounds. These are relatively low-cost and easy to process materials that intrinsically exhibit good electrical transport properties and tunable thermal transport properties with site substitutions.[2,5,9–16] Skutterudites have the space group Im3 and consist of cage-like structures with the general formula A_4B_{12} where A is a transition metal and B is a pnictogen. Figure 1 shows the crystal structure of a filled skutterudite featuring M filler atoms and B rings in an A lattice, where M = La, Te, Ge, Ba, In, or Yb; A = Fe, Ru, Co, Ni, or Os; B = Sb, P, or As. Skutterudite compounds generally have a ZT value around 1 and maintain large carrier concentrations and moderate Seebeck coefficients.[17,18] The incorporation of filler atoms reduces its thermal conductivity through the "rattling motion." Alkaline earths have previously been used as fillers[5] and Yang *et al.*[19] have shown that a double-filled skutterudite, having one alkaline earth and one lanthanide (Ba and Ce) filler, is even more effective at reducing the lattice thermal conductivity than using two alkaline earths (Ba and Sr). The combination of Ca and Ce used in this report mimics this approach but for elements with greater mass difference (71% mass difference compared to just 2%). The structure of a skutterudite also has large degrees of freedom for doping and alloying. This makes it attractive for customization and design studies.

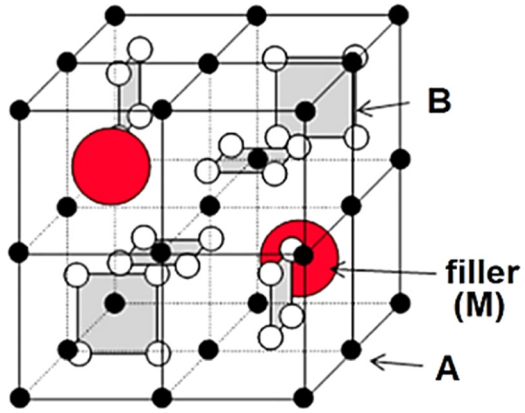

FIG. 1. Crystal structure of a filled $M_2A_8B_{24}$ skutterudite with filler atom M in red, B in white, and A in black. The gray substructures outlined by B atoms are referred to as pnictogen rings.

In addition to incorporating filler atoms, substituting B sites with different species is another approach to improve the *ZT* value. Cobalt triantimonide ($CoSb_3$) is a skutterudite of particular interest for power generation because it can operate at high temperatures (≈900 K). Substitutions that have been investigated for the $CoSb_3$ structure include Cr,[20] Ni,[21] or Fe[22] on the Co site, and Ge or Te on the Sb site. These substitutions reveal significant changes in transport properties such as an increase in electrical conductivity and a decrease in thermal conductivity. Therefore, a fundamental investigation of fillers and substitutions and their effects on the thermoelectric properties of skutterudite compounds is important for materials development.

As a follow-up to our previous work,[22] this paper investigates the effect of Ca/Ce filler atoms in Fe_4Sb_{12} and Te/Ge substitutions on the Sb site in Co_4Sb_{12}. The stoichiometry for the Ca/Ce double-filled system follows the form $CaCeFe_8Sb_{24}$ but the proper ordering of the Ca and Ce atoms follows that of Figure 2 which requires a supercell of $Ca_4Ce_4Fe_{32}Sb_{96}$ to describe the system. In $Co_4Sb_{12-2x}Te_xGe_x$, six compositions are considered where $x = 0$, 0.5, 1, 2, 3, and 6. This range of compositions offers a complete look at the substitution up to a complete replacement of the Sb atoms ($Co_4Te_6Ge_6$). To investigate the atomic structure features, we calculated the lattice constant, *a*, for the $Ca_{0.5}Ce_{0.5}Fe_4Sb_{12}$ system and lattice constant, *a*, and cell angle, *γ*, as a function of *x* for the $Co_4Sb_{12-2x}Te_xGe_x$ system. The atomic, electronic, and phonon dispersion effects were also investigated for each compound. This work helps identify the (Fe,Co)Sb_3-type compounds with a stable structure and optimized electrical and thermal conductivity properties, hence their improved *ZT* values.

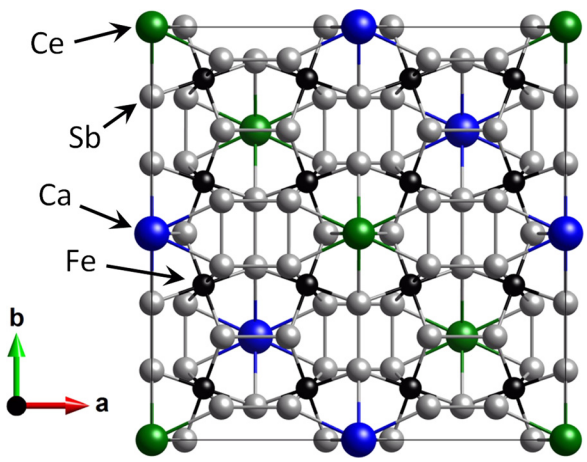

FIG. 2. Schematic of the $Ca_4Ce_4Fe_{32}Sb_{96}$ crystal structure where Ca (blue), Ce (green), Fe (black), and Sb (gray) atoms are represented by spheres. The preferred ordering of the filler atoms is to arrange all Ca atoms along (220) planes and all Ce atoms along (110) planes in this 4 × 4 × 2 supercell.

COMPUTATIONAL METHODS

Crystal structure and electronic structure calculations were performed within the density functional theory (DFT) through implementation of the Vienna *ab-initio* software package (VASP) code.[23,40] The spin-dependent generalized gradient approximation (GGA) functional was used with the Perdew-Burke-Ernzerhof (PBE) formalism.[24] Projector-augmented wave (PAW) pseudopotentials were employed with a plane wave expansion cutoff of 500 eV and a 6 × 6 × 6 Γ-centered *k*-point mesh for Brillouin zone integration.[25,26] Fermi surface broadening was accounted for by a Gaussian smearing of 0.05 eV for the $FeSb_3$ structures while 0.025 eV was used for the $CoSb_3$ structures. Atomic positions and lattice vectors were relaxed until the residual forces were reduced to less than 0.01 eV/Å. Electronic structure calculations, including density of states (DOS) and band structure calculations, were carried out on the DFT-optimized structures. A larger k-point mesh of 12 × 12 × 12 was used for the Brillouin zone integration. These calculations were performed in order to investigate the effects of Ca/Ce fillers and Te/Ge-Sb substitution on the electrical conductivity of the systems. Strong correlation effects were also tested via the DFT + U scheme for the Fe atoms and Co atoms (on-site Coulomb potential $U_{Fe} = 4.5$ eV and $U_{Co} = 7.8$ eV; exchange potential $J_{Fe} = 0.89$ eV and $J_{Co} = 0.92$ eV).[27] This approach is often used to correct the band gap which is underestimated with DFT alone.

To estimate the thermal properties of each system, density functional perturbation theory (DFPT) was used to calculate the necessary force constants by means of the Parlinski-Li-Kawazoe method.[28] The phonon density of states and phonon dispersion relations were then generated using the PHONOPY software package.[29] Force constant calculations were performed using an energy cutoff of 400 eV and a k-mesh of 1x1x1 for each structure. To account for long-range phonon interactions, a supercell convergence test was performed for each of the $Co_4Sb_{12-2x}Te_xGe_x$ structures.

RESULTS

Structural effects

The skutterudite $FeSb_3$-type crystal structure is cubic, having the space group Im3, and consisting of Fe and Sb at A and B sites, respectively (Figure 1). It has a cage-like structure with two icosahedral voids filled with guest atoms M. Previous work indicated that Ca and Ce atoms as fillers with a 1:1 ratio form $Ca_{0.5}Ce_{0.5}Fe_4Sb_{12}$ compound and exhibit a

higher *ZT* value than that of other $(Ca_xCe_{1-x})Fe_4Sb_{12}$ compounds where x = 0, 0.25, 0.75, and 1.[22] This is the consequence of large mass difference between Ca and Ce, generating a wider range of resonant rattling frequencies and leading to phonon scattering enhancement and thermal conductivity decrease.

This paper further studies the $Ca_{0.5}Ce_{0.5}Fe_4Sb_{12}$ compound. DFT structural calculations indicate a decrease in lattice constant from 9.1805 Å for the unfilled compound to 9.1777 Å (~0.03%) for the double-filled compound, which agrees well with the experimental lattice constant of 9.149056 Å for $Ca_{0.5}Ce_{0.5}Fe_4Sb_{12}$. As shown in Figure 2, a large 136 atom 4 × 4 × 2 supercell (i.e., $Ca_4Ce_4Fe_{32}Sb_{96}$) was used where the Ca and Ce were arranged with each occupying alternating (110) planes (defined using the 2 × 2 × 2 supercell). The structure has average Ca-Sb and Ce-Sb bond lengths of 3.353 Å and 3.361 Å, respectively; Sb-Ca-Sb bond angles of 52.00° and 66.85°; and Sb-Ce-Sb bond angles of 52.09° and 66.82°.

The effects of B-site substitution in skutterudites were also investigated using the $CoSb_3$ system where two Sb atoms are incrementally replaced with Te and Ge atoms, resulting in the formula $Co_4Sb_{12-2x}Te_xGe_x$, where x = 0, 0.5, 1, 2, 3, and 6. Our optimized crystal structures and calculated lattice constants, *a*, were compared with experimental values, determined by the Rietveld refinement technique and a Rietveld pattern decomposition technique.[30,31] Table I shows the calculated and experimental lattice parameters for $Co_4Sb_{12-2x}Te_xGe_x$ to illustrate the structural effects of B-site substitutions Te/Ge. The lattice constant *a* appears to decrease almost linearly as *x* increases, with the exception of *x* = 2. This is consistent with Vegard's law.[32,33] These results are expected, given that the covalent radius of Sb (1.40 Å) is larger than that of the substituents Te (1.36 Å) and Ge (1.21 Å).[34] Cell angle γ slightly shrinks at *x* = 0.5, 1, and 3, but it enlarges at *x* = 6. These changes indicate that the symmetry of the $Co_4Sb_{12-2x}Te_xGe_x$ compound is no longer perfectly cubic with Te/Ge substitution. Our DFT results agree well with experimental XRD structural analysis results (<1.0% error).

In order to better understand the atomic structures, we measured the distances between Co atoms and the rings consisting of Sb/Te/Ge. In experiments, the Co-Sb/Te/Ge distance decreases from 2.53 Å to 2.49 Å as *x* increases from 0 to 3. While the average Sb/Te/Ge-Sb/Te/Ge distances in the 4-member rings also decreases from 2.91 Å to 2.86 Å, they are longer than the typical Sb-Sb distance of 2.80 Å.[34] DFT calculations reveal that the average Co-Sb/Te/Ge bond distances decrease from 2.54 Å to 2.47 Å from *x* = 0 to 3 and even further decreased to 2.41 Å at *x* = 6, which is consistent with experimental results. From *x* = 0.5 to 2, the Co-Ge bond distance is the shortest compared to the Co-Sb and Co-Te bonds. However, in the *x* = 3 compound, the Co-Te bond distance decreases rapidly and becomes the shortest. Te/Ge substitution at *x* = 3 results in a unique structure. Due to different Co-Sb/Te/Ge bond distances and large Te/Ge substitution concentration, the 4-member rings consisting of Sb/Te/Ge are distorted, and turn into the parallelogram rings shown in Figure 3. The distortions depend on the concentration of Te/Ge substitution in the rings. Its angles range from 83° to 93°.

TABLE I. Calculated cell angle γ in degrees and lattice parameter ***a*** in units of Å for $Co_4Sb_{12-2x}Te_xGe_x$ (*x* = 0, 0.5, 1, 2, 3, and 6). The experimentally determined lattice parameter ***a**** and the percent error between calculated and experimental values is also given (* denotes experimental values).[31]

x	γ (deg)	a (Å)	a* (Å)	Error %
0	90	9.11086	9.03662	0.82
0.5	89.90	9.08122	9.01633	0.72
1	89.83	9.06154	8.99555	0.73
2	90	8.88705	8.94781	−0.68
3	89.96	8.96417	8.89584	0.77
6	90.26	8.79712	…	…

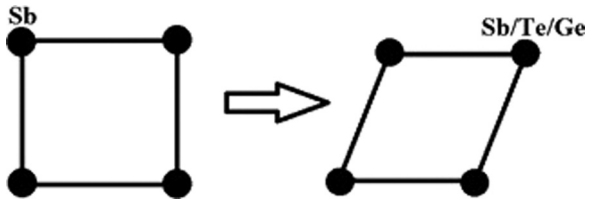

FIG. 3. Model depicting pnictogen rings within the filled skutterudite structure. Upon Te/Ge substitution, the ring distorts to an angle of up to 83° for $Co_4Sb_{12-2x}Te_xGe_x$ at *x* = 3.

Electrical properties

The Ca and Ce filler atoms in $FeSb_3$ affect the electronic structure as well as the crystal structure. As shown in Figure 4, the electronic DOS for the Fe_8Sb_{24} structure shows that the material is already electronically conductive because, at

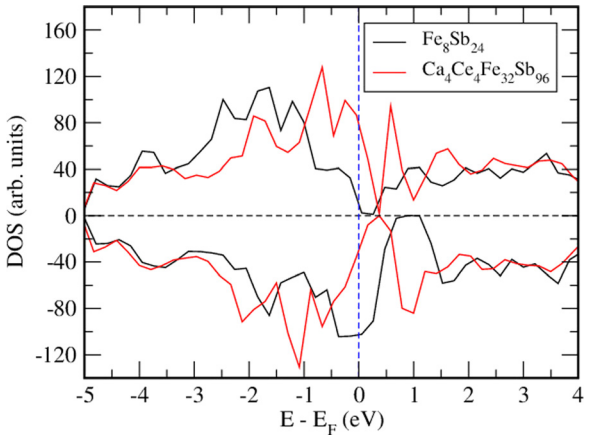

FIG. 4. Electronic density of states for the unfilled (black line) and CaCe-filled (red line) $FeSb_3$ structure. In order to account for the correct Ca-Ce ordering as shown in Figure 2, a large $Ca_4Ce_4Fe_{32}Sb_{96}$ supercell structure was used. For the sake of comparison, the DOS magnitude for the unfilled structure is increased by a factor of four. Dotted lines depict the zero values on both axes and the x-axis is shifted so the zero-point represents the Fermi level (depicted by the blue dotted line). The up- and down-spin DOS are given by positive and negative values, respectively. The difference in shape between spin-up and spin-down is primarily caused by the magnetism of the Fe atoms in the system. The unfilled Fe_8Sb_{24} (black) results show a band gap only for the positive DOS while neither the up- nor down-spin CaCe-filled (red) DOS has a significant band gap.

the Fermi level, there is low DOS for the spin-up (positive y-values) and relatively large DOS for the spin-down. The difference in spin-up and spin-down DOS is caused by the magnetism of Fe in the system. The Ca/Ce-filled structure, having the proper Ca-Ce ordering as shown in Figure 2, is also electronically conductive but with a more subtle difference between spin-up and spin-down DOS than the unfilled structure. Experimentally, it is shown that this particular Ca-Ce ordered structure is not necessarily the most electronically conductive type of Ca/Ce-filled $FeSb_3$ but is conductive enough to allow for high ZT values.[22] Indeed, in Figure 4 the presence of a zero-DOS point near the Fermi level could indicate potential for this material to exhibit semi-metallic behavior.

Similarly, the electronic conductivity for the $CoSb_3$ structure is affected by the concentration of Te/Ge substitution. Through electronic structure calculations, we studied the Te/Ge substitution effect on the band gap of each $Co_4Sb_{12-2x}Te_xGe_x$ compound ($x = 0$, 0.5, 1, 2, and 3), which allowed us to predict the electrical conductivity change. Comparison with experimental data validated the computational prediction.[30] Further studies of local density of states provided insight into Co-Te/Ge bonding.

Figure 5(a) shows DOS for $Co_4Sb_{12-2x}Te_xGe_x$. Fermi energy is shifted to 0 eV. At $x = 0$, the compound is semiconducting with a band gap of $\approx$0.16 eV. As x increases to 0.5, the band gap decreases. Interestingly, when Te/Ge concentration continues increasing, the band gap first opens wider but then completely closes at $x = 3$. Such band gap changes reveal the affect of Te/Ge substitution on the electrical conductivity of the compound. The compound at $x = 0$ is expected to have the smallest electrical conductivity while the highest electrical conductivity occurs at $x = 3$ due to no band gap. From $x = 0.5$ to 1, the electrical conductivity should slightly decrease due to the wider band gap. These computational predictions are consistent with experimental measurements which show that increasing Te concentration in Ge-doped $CoSb_3$ increases the electrical conductivity.[35,36]

We further studied the local DOS (LDOS), which projected the density on each metal site. Through this approach, the density of states can be split into contributions from each individual atom. When these corresponding plots overlap, it suggests that each atom is contributing to the density of states at that given energy level, implying orbital hybridization. Figure 5(b) illustrates the orbital hybridization through the energy bands of -13 eV to 5 eV between Co and Te/Ge substitution at $x = 0.5$. It indicates the covalent characteristics of Co-Te/Ge bonds due to the overlap of orbital energies. As Te/Ge substitution concentration increases, the average Co-Te/Ge bond distances decrease because of its stronger covalent characteristics.

Further analysis of band alignment facilitates the engineering of the skutterudite compounds for specific thermoelectric applications. The band structures of $Co_4Sb_{12-2x}Te_xGe_x$ for $x = 0$, 0.5, and 3 were calculated along lines connecting high-symmetry points in the Brillouin zone as shown in Figure 6. The perfect $CoSb_3$ ($x = 0$) is a direct band gap semiconductor with a calculated gap of 0.16 eV. The valence band maximum (VB_{max}) and conduction band minimum (CB_{min}) are both located at the Γ point. There also exists an indirect gap between some lower-symmetry point having a local maximum between M and Γ that is separated from the CB_{min} by 0.50 eV. As Te/Ge substitutions are introduced ($x = 0.5$), the material remains a direct band gap semiconductor but with a narrower size of 0.13 eV. This is caused by the decrease in CB_{min} at the Γ point from 0.084 eV to 0.066 eV. Also, the local maximum at the M point increases (from -0.536 eV to -0.355 eV), giving rise to a shorter indirect gap of 0.42 eV that now exists from M $\rightarrow$ Γ high-symmetry points. This implies that with adjusting x values, the compound could shift from a direct to an indirect band gap semiconductor, creating more potential applications for the compounds. To confirm our prediction, we observed $x = 3$ (Figure 6(c)) which shows the smaller band gap of 0.11 eV, suggesting a high electrical conductivity. Both the VB_{max} peak and CB_{min} trough at the Γ point split, forming an indirect gap.

The electronic structure results indicate a strong Te/Ge substitution dependence in $Co_4Sb_{12-2x}Te_xGe_x$, motivating us to investigate further increasing x to the full substitution of Sb with Te/Ge ($x = 6$ or $Co_4Te_6Ge_6$). Figure 7 shows

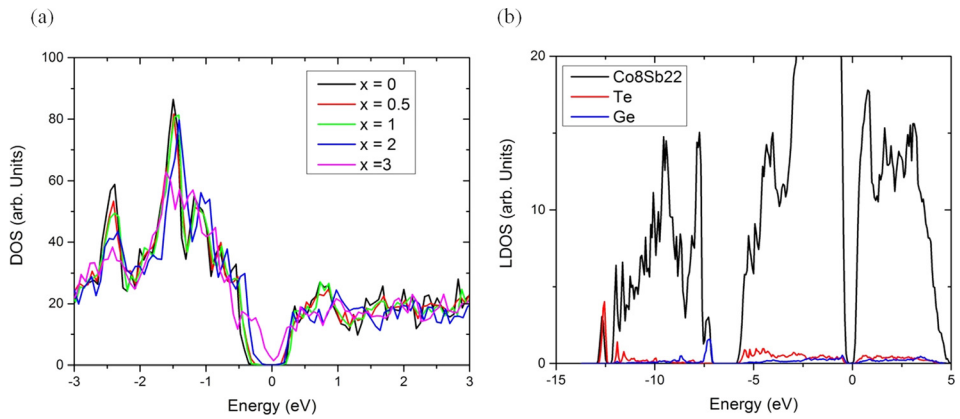

FIG. 5. Electronic density of states (DOS) for $Co_4Sb_{12-2x}Te_xGe_x$, Fermi energy = 0: (a) Total DOS for $x = 0$, 0.5, 1, 2, and 3; and (b) local DOS (LDOS) for Co_8Sb_{22} (black), Te (red), and Ge (blue) in $Co_8Sb_{22}TeGe$ (i.e., $Co_4Sb_{11}Te_{0.5}Ge_{0.5}$ with $x = 0.5$). DOS results in (a) indicate that the band gap decreases with increasing x. Part (b) shows an interaction between the local Te and Ge densities indicating orbital hybridization. This implies covalent characteristics of the Co-Te/Ge bonds which could explain the decreased Co-Te/Ge bond distances.

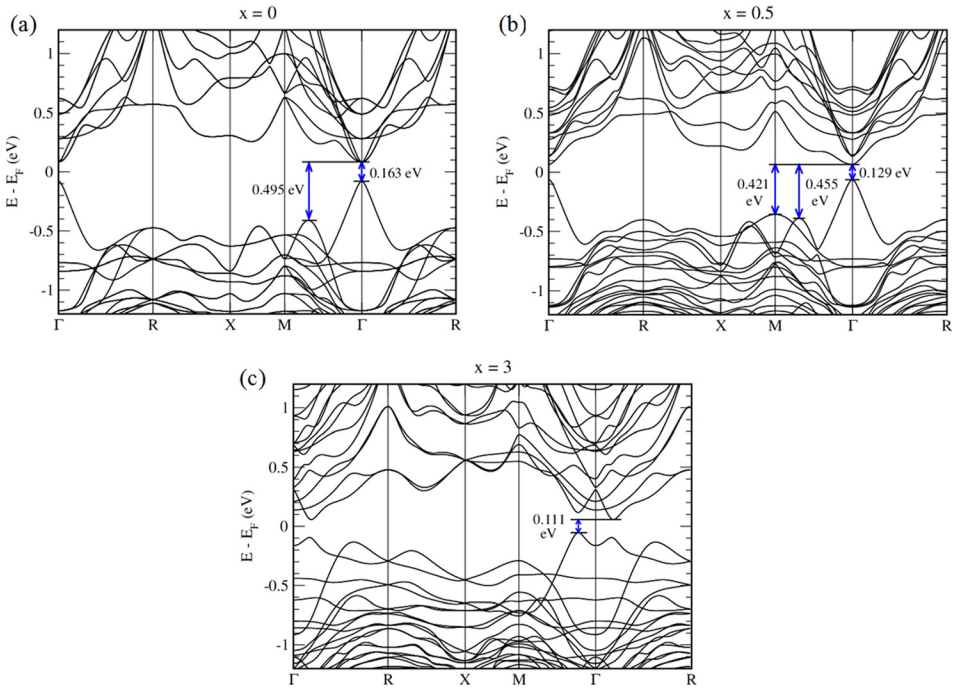

FIG. 6. Electronic band structure diagrams of $Co_4Sb_{12-2x}Te_xGe_x$ for (a) $x=0$, (b) $x=0.5$, and (c) $x=3$. Blue arrows indicate the changes in the direct and indirect band gaps. As substitution increases, the band gap decreases from (a) 0.16 eV to (b) 0.13 eV, and eventually to (c) 0.11 eV for the highest doped structure investigated ($x=3$). Also note the transition from direct to indirect band gap semiconducting behavior in part (c).

electronic DOS for $x=6$ (full substitution) in comparison with that for $x=3$ (half substitution) and different atomic arrangements for Sb, Te, and Ge. In Figure 7(b), the black line depicts the electronic DOS for $x=6$, where there is no band gap and the local minimum in DOS at the Fermi level also has a higher value than that of $x=3$ (see Figure 7(a)). This suggests a generally increasing conductivity with increasing x. Interestingly, we found that atomic arrangements for Sb, Te, and Ge in the pnictogen rings affect the band gap size. As seen in Figure 7(c), configuration 1 involves the least amount of "order" where the Sb, Te, and Ge atoms are randomly arranged throughout the Sb sites.

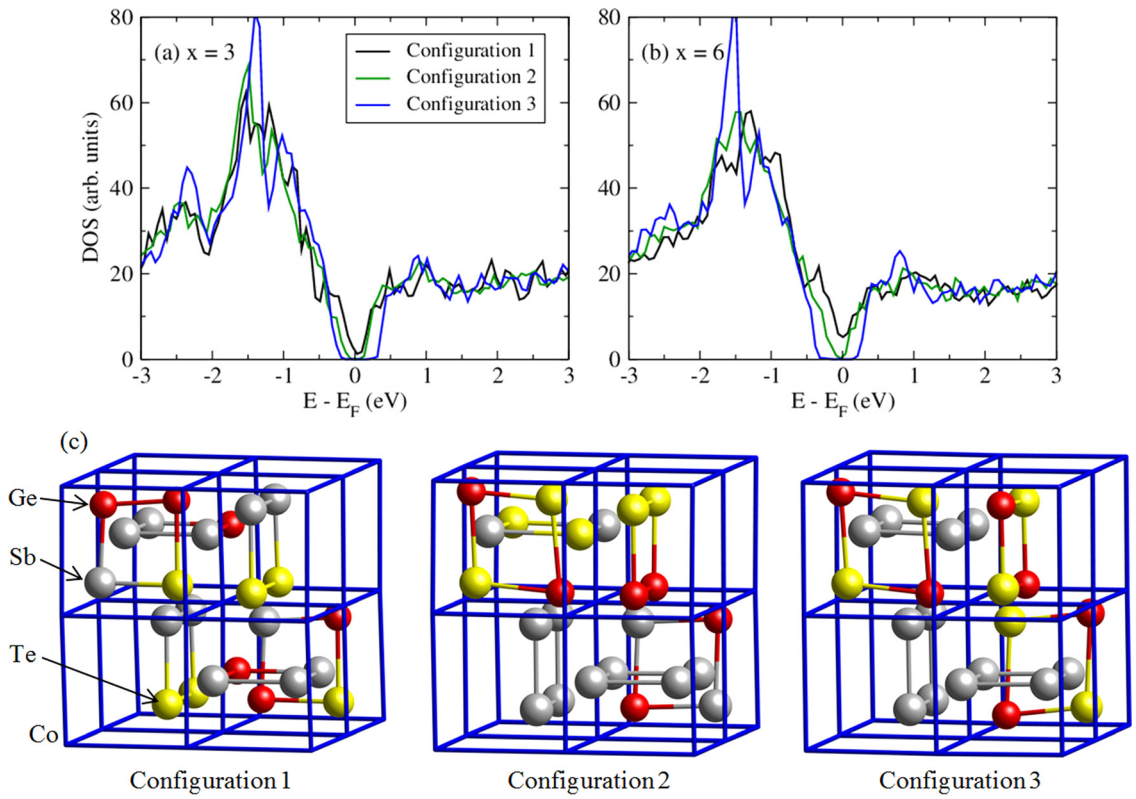

FIG. 7. Density of states plots for $Co_4Sb_{12-2x}Te_xGe_x$ where (a) $x=3$ and (b) $x=6$. Fermi energy is zero. The black, green, and blue plots depict the randomly ordered (configuration 1), the partially ordered (configuration 2), and fully ordered (configuration 3) pnictogen ring configurations. The pnictogen ring ordering increasingly opens up the band gap. An example of each pnictogen ring configuration (depicted using the $x=3$ structure) is shown in part (c) where the blue line shows Co-Co bonds and the gray, yellow, and red spheres depict Sb, Te, and Ge atoms, respectively.

This is the configuration used for all substituted structures in Figure 5(a). Ordering refers to having some pnictogen rings composed of entirely Sb and/or having some only 2Te/2Ge rings arranged such that the Te and Ge atoms are at alternating sites around the ring. Configuration 2 is an example of this for the $x = 3$ system. Finally, configuration 3 involves no randomly ordered rings, demonstrating that all Sb atoms are only sharing Sb rings at $x = 3$ and all Te and Ge atoms are only sharing 2Te/2Ge rings arranged as explained above. As a result, pnictogen ring "ordering" increases from configuration 1 to configuration 3. We found that increasing the ring ordering opens up a band gap (green line) and further increases the gap (blue line) to as much as 0.32 eV and 0.33 eV for $x = 3$ and $x = 6$, respectively (see Figures 7(a) and 7(b)). Our computational results emphasize the importance for understanding the atomic structure of these materials and the atomic structure-electrical property relationships.

Phonon properties

The scattering of phonon modes in a material hinders thermal transport, which results in reduced lattice thermal conductivity κ_l. There are a variety of methods for increasing phonon scattering, including nanostructuring, alloying, introducing more disorder or interfaces, and changing the structure or composition.[37] By analyzing the phonon dispersion relations of a material, one can estimate the effects of fillers or substitutions on the resulting lattice thermal conductivity. For example, the phonon group velocity $v_{k\lambda}$ can be estimated by observing the slopes or gradients of the phonon dispersion data through the equation

$$v_{k\lambda} = \frac{\partial \omega}{\partial k}, \tag{1}$$

where ω is the phonon frequency and k is the wave vector. The phonon group velocity is then related to the lattice thermal conductivity through the following equation:

$$\kappa_l = \frac{1}{3VN_k} \sum_{k\lambda} c_{k\lambda} v_{k\lambda}^2 \tau_{k\lambda}, \tag{2}$$

where V is the volume of the unit cell, N_k is the number of k-points, c is the heat capacity, and τ is the phonon relaxation time for the given phonon branch, λ.[38,39] From this, the lattice thermal conductivity can be estimated qualitatively by analyzing the slope of the phonon dispersion results. Figure 8 shows phonon density of states data for the large 136-atom $Ca_4Ce_4Fe_{32}Sb_{96}$ compound compared to that of Fe_8Sb_{24}. Phonon dispersion data were also calculated but due to the large number of modes ($136 \times 3 = 408$ modes) for the CaCe-filled system, the results were more clearly displayed via the phonon density of states instead. We found that the incorporation of Ca and Ce filler atoms broadens the phonon bands, implying an increase in phonon scattering typically observed in filled skutterudite systems. The optical modes are also significantly flatter than the acoustic modes, indicating that the lattice thermal conductivity for this material is dominated by the acoustic modes.

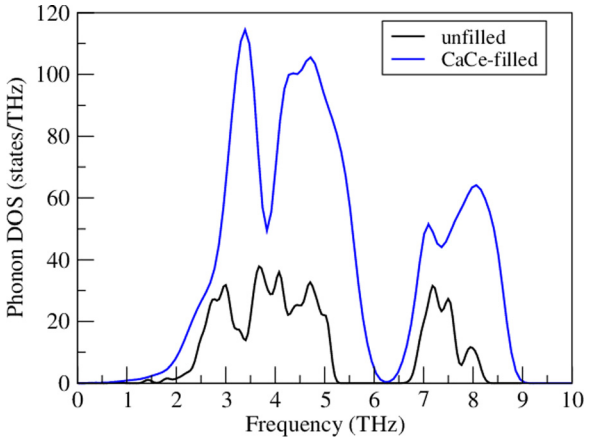

FIG. 8. Phonon density of states for unfilled Fe_8Sb_{24} (black) and CaCe-filled $Ca_4Ce_4Fe_{32}Sb_{96}$ (blue). To account for the proper Ca/Ce filler atom ordering which provides the most stable structure (and most promising thermoelectric performance) of the $Ca_{0.5}Ce_{0.5}Fe_4Sb_{12}$ system, the larger 136-atom supercell was used for the "CaCe-filled" structure.

Similarly, the effects of substitution on lattice thermal conductivity were also estimated by analyzing the phonon properties. Figure 9(a) shows the phonon dispersion relation for the $Co_4Sb_{12-2x}Te_xGe_x$ compound at $x = 0$. Figure 9(b) compares the acoustic modes for the $Co_4Sb_{12-2x}Te_xGe_x$ compounds at $x = 0$, 3, and 6, where the x-axes for each data set is normalized to the values of the compound at $x = 6$ (for the purpose of comparison). The compound at $x = 3$ has the lowest phonon dispersion gradient, so it should exhibit the lowest lattice thermal conductivity. Figure 9(c) compares the phonon density of states for the three compounds. It shows a broadening of the phonon bands, particularly for the higher-frequency band, for the compounds with Te and Ge substitutions at $x = 3$ and 6. Ge substitutions contribute to the higher frequency modes since Ge has a lower atomic weight than Sb. In contrast, the modes at the lower frequencies are associated with the heavier Te substitutions. $x = 0$ exhibits a sizable gap between the higher-frequency band and the lower band. As substitution increases, this gap decreases and is eventually eliminated at $x = 6$. This spreading of optical modes indicates a reduction in lattice thermal conductivity. For either $x = 3$ or $x = 6$, the optical modes are significantly flatter than the acoustic modes, suggesting that the lattice thermal conduction is likely dominated by the acoustic modes in these compounds.

CONCLUSION

We have investigated the crystal structures, electrical properties, and thermal properties of filled $Ca_{0.5}Ce_{0.5}Fe_4Sb_{12}$ and substituted $Co_4Sb_{12-2x}Te_xGe_x$ compounds ($x = 0$, 0.5, 1, 2, 3, and 6) using a DFT-based approach. The stable Ca/Ce ordering required the use of a large $Ca_4Ce_4Fe_{32}Sb_{96}$ supercell with each filler atom occupying alternating (110) planes. For the $Co_4Sb_{12-2x}Te_xGe_x$ compounds, structural distortion occurs with Te/Ge substitution. At $x = 3$ (i.e., 1:1 Sb:Te/Ge ratio) four-member pnictogen square rings have the largest distortion and become parallelograms with an angle of 83°.

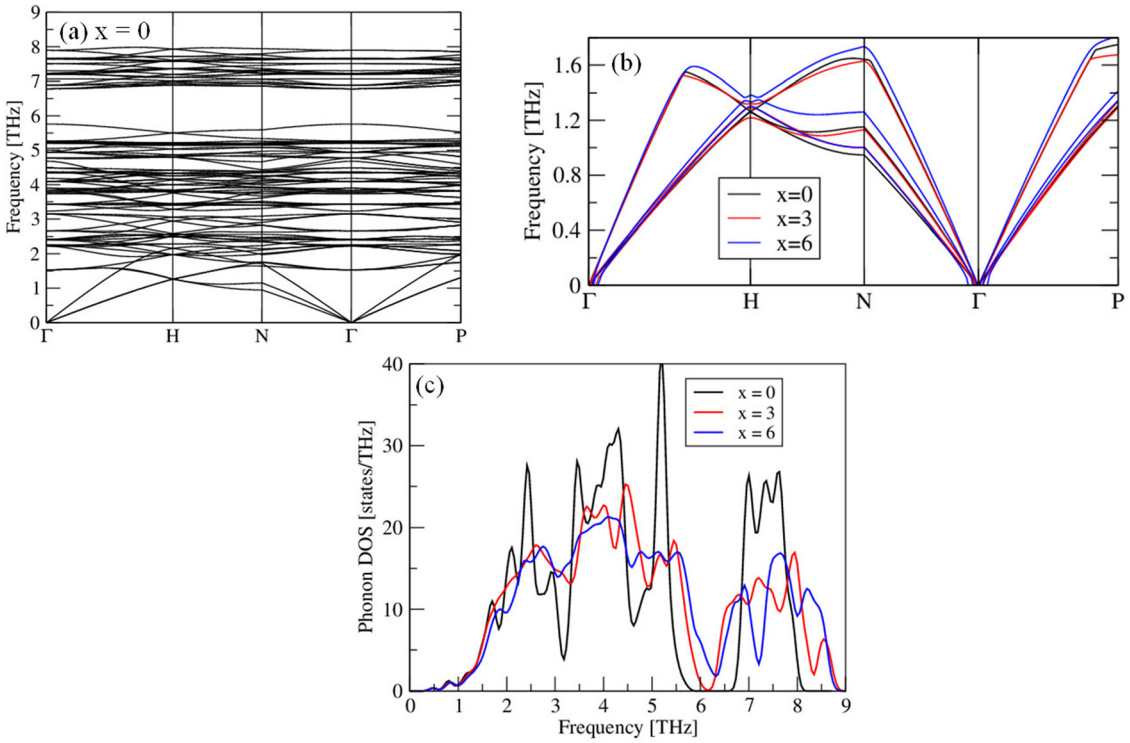

FIG. 9. Phonon property calculations. (a) Phonon dispersion relation for $Co_4Sb_{12-2x}Te_xGe_x$ at x = 0. Similar plots were made for $x = 3$ and $x = 6$ but for brevity, only their acoustic modes (along with those of $x = 0$) are given in (b), and (c) total phonon density of states for each compound, projected across the full range of mode frequencies.

Electronic structure calculations indicate that the Ca/Ce double-filled $FeSb_3$ is conductive with no band gap. The band gap of $Co_4Sb_{12-2x}Te_xGe_x$ varies with Te/Ge substitution concentration leading to a reduction in band gap and therefore an increase of electrical conductivity. The covalent characteristics of Co-Te/Ge bonds account for orbital hybridizations between Co and Te/Ge. Band structures exhibit the change of band alignments near the Fermi energy as x increases. At $x = 3$, the compound transfers from a direct to indirect band-gap semiconductor. We also found a strong correlation between the ordering/configuration of pnictogen rings and the electronic band gap for these compounds. We predicted the thermal conductivity change through the analysis of phonon density of states and phonon dispersion relations for the compounds. The phonon bands are broadened with the incorporation of either fillers or substitutions. Lattice thermal conductivity change is controlled by the acoustic phonon modes in both cases. For the $Co_4Sb_{12-2x}Te_xGe_x$ compounds, phonon scattering and acoustic mode gradient change are evident as substitution increases. The compound at $x = 3$ is expected to have the lowest lattice thermal conductivity. Our work exhibits improved thermoelectric properties via filler and substitutional doping. More work will be conducted to confirm the predictions through further *ZT* calculations and experimental measurements.

ACKNOWLEDGMENTS

This work was partially supported by the NSF EAPSI Fellowship Grant No. 1414593. Computing facilities were provided by Boise State University's R1 cluster, and Idaho National Laboratory's high performance computing (HPC) center. The authors thank Dr. Jin Zhao at the University of Science and Technology of China for helpful discussions.

[1]L. Bjerg, G. K. H. Madsen, and B. B. Iversen, Chem Mater. **23**, 3907 (2011).
[2]G. J. Tan, S. Y. Wang, H. Li, Y. G. Yan, and X. F. Tang, J. Solid State Chem. **187**, 316 (2012).
[3]K. Chrissafis and D. Bikiaris, Thermochim. Acta **523**, 1 (2011).
[4]D. Dragoman and M. Dragoman, Appl. Phys. Lett. **91**, 203116 (2007).
[5]J. S. Dyck, W. D. Chen, C. Uher, L. Chen, X. F. Tang, and T. Hirai, J. Appl. Phys. **91**, 3698 (2002).
[6]D. D. Freeman, K. Choi, and C. Yu, PLoS One **7**, e47822 (2012).
[7]Y. Zhao, G. S. Tang, Z. Z. Yu, and J. S. Qi, Carbon **50**, 3064 (2012).
[8]Y. Lan, A. J. Minnich, G. Chen, and Z. Ren, Adv. Funct. Mater. **20**, 357 (2010).
[9]W. Wong-Ng, J. A. Kaduk, G. Tan, Y. Yan, and X. Tang, Powder Diffr. **29**, 260 (2014).
[10]G. J. Tan, W. Liu, H. Chi, X. L. Su, S. Y. Wang, Y. G. Yan, X. F. Tang, W. Wong-Ng, and C. Uher, Acta Mater. **61**, 7693 (2013).
[11]Y. G. Yan, W. Wong-Ng, J. A. Kaduk, G. J. Tan, W. J. Xie, and X. F. Tang, Appl. Phys. Lett. **98**, 142106 (2011).
[12]T. He, J. Z. Chen, H. D. Rosenfeld, and M. A. Subramanian, Chem. Mater. **18**, 759 (2006).
[13]B. Huang and M. Kaviany, Acta Mater. **58**, 4516 (2010).
[14]R. Hara, S. Inoue, H. T. Kaibe, and S. Sano, J. Alloys Compd. **349**, 297 (2003).
[15]H. Kim, M. Kaviany, J. C. Thomas, A. Van der Ven, C. Uher, and B. L. Huang, Phys. Rev. Lett. **105**, 265901 (2010).
[16]P. F. Luo, X. F. Tang, C. Xiong, and Q. J. Zhang, Acta Phys. Sin-Ch. Ed. **54**, 2403 (2005).
[17]D. T. Morelli, T. Caillat, J. P. Fleurial, A. Borshchevsky, J. Vandersande, B. Chen, and C. Uher, Phys. Rev. B **51**, 9622 (1995).
[18]T. Caillat, A. Borshchevsky, and J. P. Fleurial, J. Appl. Phys. **80**, 4442 (1996).
[19]J. Yang, W. Zhang, S. Q. Bai, Z. Mei, and L. D. Chen, Appl. Phys. Lett. **90**, 192111 (2007).

[20]J. Yang, M. G. Endres, and G. P. Meisner, Phys. Rev. B **66**, 014436 (2002).
[21]J. Yang, D. T. Morelli, G. P. Meisner, W. Chen, J. S. Dyck, and C. Uher, Phys. Rev. B **65**, 094115 (2002).
[22]Y. G. Yan, W. Wong-Ng, L. Li, I. Levin, J. A. Kaduk, M. R. Suchomel, X. Sun, G. J. Tan, and X. F. Tang, J. Solid State Chem. **218**, 221 (2014).
[23]G. Kresse and J. Furthmuller, Phys. Rev. B **54**, 11169 (1996).
[24]J. P. Perdew, K. Burke, and M. Ernzerhof, Phys. Rev. Lett. **77**, 3865 (1996).
[25]P. E. Blöchl, Phys. Rev. B **50**, 17953 (1994).
[26]G. Kresse and D. Joubert, Phys. Rev. B **59**, 1758 (1999).
[27]A. I. Liechtenstein, V. I. Anisimov, and J. Zaanen, Phys. Rev. B **52**, R5467 (1995).
[28]K. Parlinski, Z. Q. Li, and Y. Kawazoe, Phys. Rev. Lett. **78**, 4063 (1997).
[29]A. Togo, F. Oba, and I. Tanaka, Phys. Rev. B **78**, 134106 (2008).
[30]X. Su, Y. Yan, W. Wong-Ng, I. Williamson, L. J.-Y. Her, J. A. Kaduk, and L. Li, "Structure and Property Relationships of the Skutterudite Series $Co_4Sb_{12-2x}Te_xGe_x$ (x = 0, 0.5, 1, 2, 3) for Thermoelectric Applications," Powder Diffr. (unpublished).
[31]H. M. Rietveld, J. Appl. Crystallogr. **2**, 65 (1969).
[32]L. Vegard, Z. Phys. **5**, 17 (1921).
[33]L. Vegard, Z. Kristallogr. **67**, 239 (1928).
[34]P. Pyykko and M. Atsumi, Chem.: A Eur. J. **15**, 186 (2009).
[35]X. L. Su, H. Li, Q. S. Guo, X. F. Tang, Q. J. Zhang, and C. Uher, J. Electron. Mater. **40**, 1286 (2011).
[36]X. L. Su, H. Li, G. Y. Wang, H. Chi, X. Y. Zhou, X. F. Tang, Q. J. Zhang, and C. Uher, Chem. Mater. **23**, 2948 (2011).
[37]G. J. Snyder and E. S. Toberer, Nat. Mater. **7**, 105 (2008).
[38]T. F. Luo, J. Garg, J. Shiomi, K. Esfarjani, and G. Chen, Europhys. Lett. **101**, 16001 (2013).
[39]J. D. Chung, A. J. H. McGaughey, and M. Kaviany, ASME Trans. J. Heat Transfer **126**, 376 (2004).
[40]Certain commercial equipment, materials, or software are identified in this paper in order to specify the experimental or computation procedure adequately. Such identification is not intended to imply recommendation or endorsement by the National Institute of Standards and Technology, nor is it intended to imply that the materials, equipment, or software identified are necessarily the best available for the purpose.